

Comparison of analytical descriptions of nocturnal low-level jets within the Ekman model framework

Elizabeth Smith¹ · Evgeni Fedorovich¹ · Alan Shapiro¹

Received: 9 August 2016 / Accepted: 12 December 2016 / Published online: 22 December 2016
© Springer Science+Business Media Dordrecht 2016

Abstract This study focuses on the inertial oscillation aspect of the nocturnal low-level jet (NLLJ). In the context of the Ekman model solutions, conceptual NLLJ inertial oscillation analytical frameworks proposed by Blackadar in 1957 and Shapiro and Fedorovich and van de Wiel et al. in 2010 are compared. Considering a NLLJ produced via direct numerical simulation over flat terrain with no baroclinic influence as a reference case, the deficiencies of each framework in representing a realistic NLLJ are assessed. The Blackadar theory results in unrealistic wind profiles near the surface. While extensions of Blackadar's framework by Shapiro and Fedorovich and van de Wiel et al. produce more realistic NLLJs, the simpler approach taken by van de Wiel et al. does not describe the NLLJ wind hodograph at later times sufficiently in qualitative terms.

Keywords Analytical model · Blackadar's theory · Low-level jet · Inertial oscillation

1 Introduction

The nocturnal low-level jet (NLLJ) is defined as a wind maximum occurring overnight in the lowest kilometer of the atmosphere. The NLLJ is frequently observed in the United States [2, 3, 5, 6, 10, 12, 13, 15, 16, 18–20], Australia, Europe, North Africa, and elsewhere in the world [1, 4, 16]. In the U.S., NLLJs commonly form over the Great Plains; these jets are typically southerly and most often occur during the warm months of late spring, summer, and early autumn. In the NLLJ climatology presented by Bonner [6], the average height of NLLJ wind maxima is about 800 m above ground level (a.g.l.). More recently, Whiteman et al. [19] showed that half of NLLJs occurring over the Great Plains have wind

✉ Elizabeth Smith
elizabeth.n.smith@ou.edu

¹ School of Meteorology, University of Oklahoma, 120 David L. Boren Blvd., Norman, OK, USA

maxima below 500 m. The NLLJ winds can be very strong, in many cases exceeding the geostrophic wind speed of the previous day by more than 70% [14].

NLLJs in the Great Plains are of meteorological importance due to their influence on weather and climate over the region [16]. Moisture transport from the Gulf of Mexico northward over the central U.S. by NLLJs has been related to the observed nocturnal maximum in warm-season rainfall recorded over the central U.S. [11]. Thermodynamic and dynamic support for the initiation of deep convection and severe weather phenomena [16] can be provided by NLLJs. Strong wind shear associated with NLLJs can be hazardous for aviation especially during takeoffs and landings. Beyond the aforementioned practical applications, NLLJs are of theoretical interest as fluid dynamical phenomenon due to the peculiarity of the physical mechanisms associated with NLLJ formation.

The dynamics of NLLJs have been described by various theories in the literature. While each theory attempts to explain particular features of the NLLJ, a theory correctly or fully describing this phenomenon as observed has yet to be developed. Blackadar [5] detailed the NLLJ as an inertial oscillation in the lower atmosphere occurring once frictional restraint from the surface is released after sunset. This oscillation results in the nocturnal wind vector turning around the geostrophic wind vector. In order to facilitate a more complete understanding of the inertial oscillation mechanism and the roles of vertical momentum transport and intra-layer friction in the NLLJ, Shapiro and Fedorovich [14] extended the Blackadar theory by considering the NLLJ as an inertial oscillation initiated by the sudden reduction of frictional constraint rather than the full release. The resulting inertial oscillation tends toward a steady-state nocturnal Ekman wind profile with reduced eddy viscosity. Finding the analytical approach of Shapiro and Fedorovich rather complicated and impractical, van de Wiel et al. [17] presented a simpler model of the NLLJ by employing constant friction rather than allowing friction to vary in time. This model produces an undamped nocturnal wind profile oscillation around an equilibrium wind profile that would exist in a stationary nocturnal boundary layer.

The present work compares the ability of the three aforementioned analytical frameworks, hereafter BLK1957 [5], SF2010 [14], and VDW2010 [17], to represent a realistic NLLJ inertial oscillation. In the following sections, each analytical framework will be evaluated against each other and against data from an idealized direct numerical simulation (DNS) of a NLLJ inertial oscillation. The frameworks will then be compared, and their strengths and weaknesses will be identified.

2 Analysis

The modern computational tool of DNS resolves turbulent motions within a prescribed scale range by directly integrating the relevant equations of boundary-layer dynamics and thermodynamics (e.g., [9]). In this study we applied this technique to produce a NLLJ over flat terrain with no baroclinic effects. The DNS code employed in this study is a close counterpart of the one described in [8] and used the following governing parameters representing external forcings: squared Brunt-Väisälä (buoyancy) frequency $N^2 = 10^{-4} \text{ s}^{-2}$, Coriolis parameter $f = 10^{-4} \text{ s}^{-1}$, kinematic viscosity $\nu = 1 \text{ m}^2\text{s}^{-1}$, and geostrophic wind components $U_g = 0 \text{ ms}^{-1}$ and $V_g = 10 \text{ ms}^{-1}$. The large scale synoptic forcing is accounted for via these geostrophic wind components. The DNS was run on a $256 \times 256 \times 384$ ($x \times y \times z$) grid with a uniform grid spacing of 4 m with periodic boundary conditions in each lateral direction. While such a domain may not capture all relevant

eddies, tests with various domain sizes indicated that these simulations appropriately produce the NLLJ mean flow structure. Test runs also showed that the employed grid provides a reasonable balance between accuracy and computational efficiency. The Reynolds number in the simulation is $\sim 10^4$ which represents weakly turbulent flow.

Daytime was considered to be comprised of the first 10,800 s of the simulation, and nighttime extended from 10,800 to 54,000 s. Boundary conditions for momentum are free-slip at the upper boundary and no-slip at the lower boundary. Boundary conditions for buoyancy are of the Neumann type at the upper boundary (buoyancy flux going to zero) and of the Dirichlet type at the lower boundary with prescribed daytime and nighttime buoyancy values of $b_{0_{day}} = 0.1 \text{ ms}^{-2}$ and $b_{0_{night}} = 0.05 \text{ ms}^{-2}$. Note that in the DNS framework the turbulent mixing coefficient, k , is not specified. Rather, the turbulence is simulated explicitly, with no need for a mixing parameterization. Hodographs of the NLLJ produced by this DNS are shown in Fig. 1. Such hodographs may be considered representative of the NLLJ phenomenon over flat terrain with a pure geostrophic forcing.

To allow for the direct comparison of oscillating wind profiles produced by each analytical framework, the same initial wind profile is imposed for each framework. Based on the work of Ekman [7], the model for the initial state is formulated in terms of the stationary, horizontally homogeneous momentum balance in the planetary boundary layer. The corresponding governing equations are written as

$$f(v - V_g) + k \frac{\partial^2 u}{\partial z^2} = 0, \tag{1}$$

$$-f(u - U_g) + k \frac{\partial^2 v}{\partial z^2} = 0. \tag{2}$$

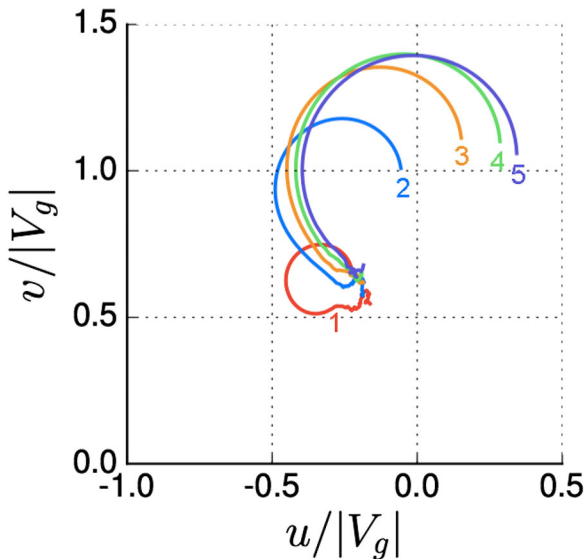


Fig. 1 Normalized hodographs show the NLLJ produced with DNS. The red line (1) represents the hodograph at 100 m a.g.l., blue line (2) at 200 m, orange line (3) at 300 m, green line (4) at 400 m, and purple line (5) at 500 m

Here, f is the Coriolis parameter, u and v are the horizontal x and y components of the mean wind, and U_g and V_g are the corresponding components of the geostrophic wind vector, assumed to be height-constant. The last terms on the left-hand sides represent the parameterized divergence of the turbulent kinematic stress using flux-gradient relationships where k is interpreted as the eddy viscosity (treated as constant in the Ekman model), and z is height above ground. The Ekman solutions for the Northern Hemisphere ($f > 0$) are

$$u = U_g - e^{-a_e z} (U_g \cos a_e z + V_g \sin a_e z), \tag{3}$$

$$v = V_g - e^{-a_e z} (V_g \cos a_e z - U_g \sin a_e z), \tag{4}$$

where

$$a_e = \sqrt{\frac{f}{2k}}.$$

Figure 2 shows Ekman model solutions with geostrophic wind components of $U_g = 0$ and $V_g = 10 \text{ ms}^{-1}$, $f = 8.7 \times 10^{-5} \text{ s}^{-1}$, and $k = 12 \text{ m}^2\text{s}^{-1}$, which may be considered representative of typical daytime conditions in the southern Great Plains. The profiles shown in Fig. 2 will be used as the initial profiles (hereafter denoted as u_0 and v_0) in further inertial oscillation calculations.

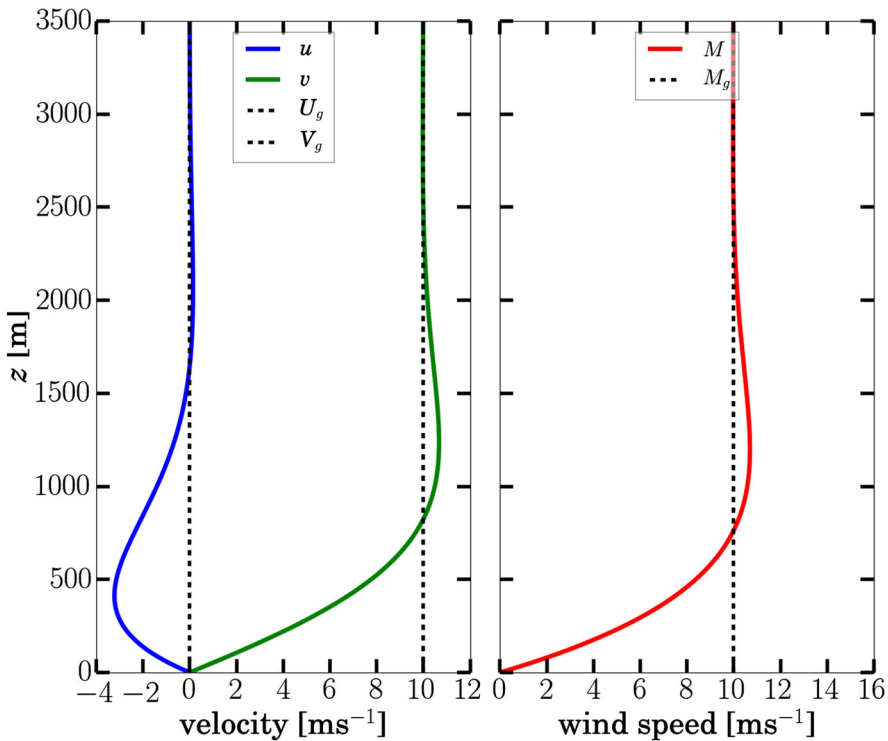


Fig. 2 Ekman model solutions in the daytime boundary layer with $U_g = 0 \text{ ms}^{-1}$ and $V_g = 10 \text{ ms}^{-1}$. The left panel shows the u - and v -components of the wind and the right panel shows the wind magnitude, $M = \sqrt{u^2 + v^2}$ with $M_g = \sqrt{u_g^2 + v_g^2} = 10 \text{ ms}^{-1}$

The BK1957 model assumes that friction (turbulent stress) goes to zero in the entire nocturnal boundary layer at sunset and remains zero throughout the night. Under this assumption, using the initial Ekman solutions profiles u_0 and v_0 , the non-stationary equations

$$\frac{\partial u}{\partial t} = f(v - V_g), \tag{5}$$

$$\frac{\partial v}{\partial t} = -f(u - U_g), \tag{6}$$

have the following oscillatory solutions:

$$u - U_g = (v_0 - V_g) \sin ft + (u_0 - U_g) \cos ft, \tag{7}$$

$$v - V_g = (v_0 - V_g) \cos ft - (u_0 - U_g) \sin ft. \tag{8}$$

The period, T , of this oscillation is $T = \frac{2\pi}{f}$ where f is the Coriolis parameter. The aforementioned value of f yields T of approximately 20 h. The top panels in Fig. 3 show the BLK1957 inertial oscillation computed over 12 h. The complete omission of friction in this model results in non-physical wind profiles near the surface as the wind speed does not go to zero at the surface. The hodograph for the BLK1957 model shows the profiles oscillating around the geostrophic wind rather than going to zero when approaching the surface.

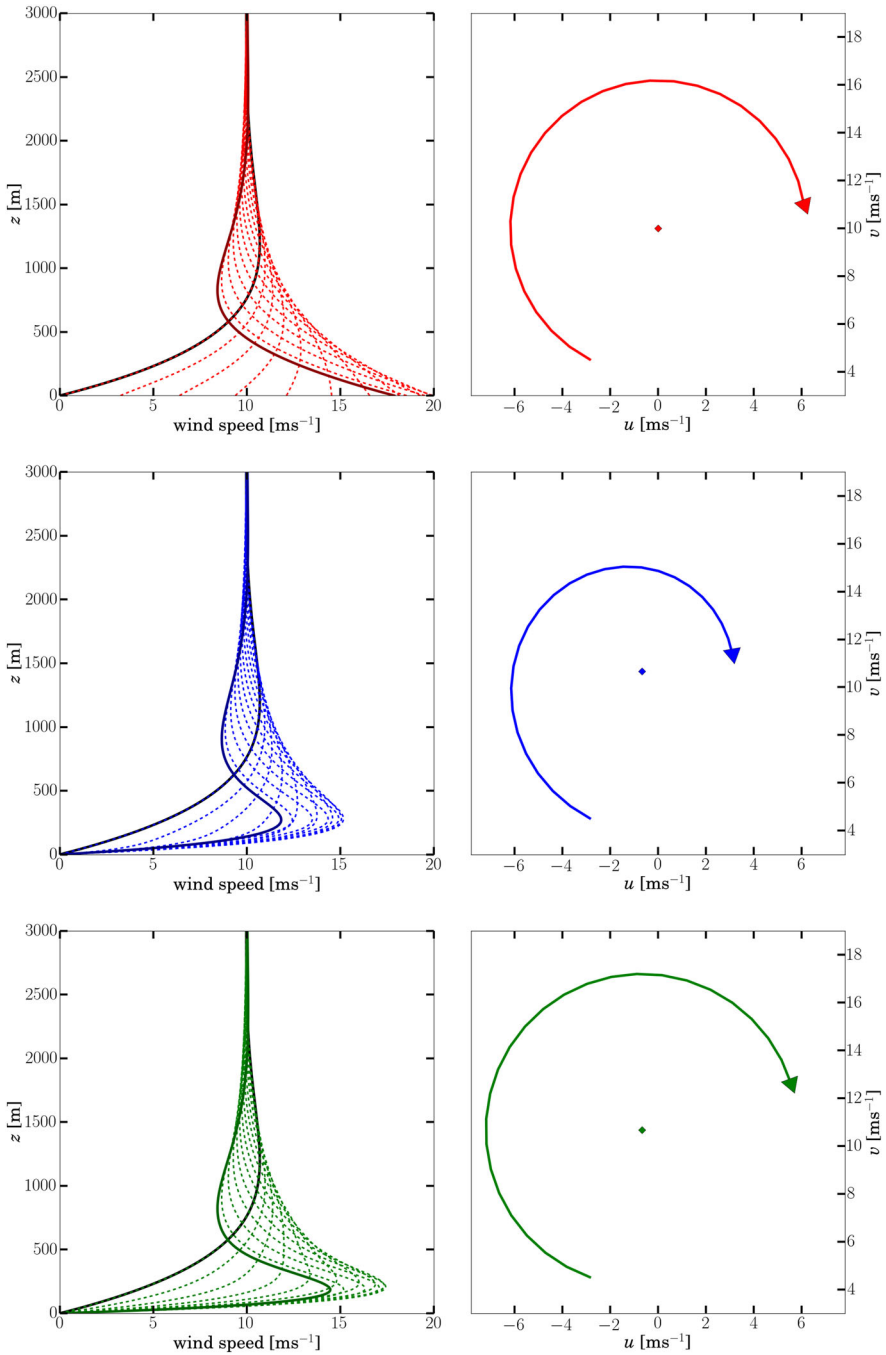
The SF2010 [14] model extends the BLK1957 framework by including frictional effects via an instantaneous drop in eddy viscosity during the transition from day to night. Employing the non-stationary momentum balance equations

$$\frac{\partial u}{\partial t} = f(v - V_g) + k \frac{\partial^2 u}{\partial z^2}, \tag{9}$$

$$\frac{\partial v}{\partial t} = -f(u - U_g) + k \frac{\partial^2 v}{\partial z^2}, \tag{10}$$

with a step-change in k at sunset, SF2010 derive an analytical solution for $u(z, t)$ and $v(z, t)$ describing the resulting inertial oscillation (the reader is directed to that work for more information). Applying the SF2010 solution with a daytime k of $12 \text{ m}^2 \text{ s}^{-1}$ and a nighttime value of $5 \text{ m}^2 \text{ s}^{-1}$ provides the oscillation shown in the middle panels of Fig. 3. The SF2010 expressions for the velocity components u and v can be found as Eqs. (36) and (37) in [14]. It is immediately apparent that the SF2010 model produces more realistic jet profiles and wind hodograph than the BLK1957 model. The wind profile produced from SF2010 goes to zero at the surface and has the low-level wind speed maximum characteristic of a low-level jet. These are both features that the wind profiles produced with BLK1957 do not have. Keeping in mind that the oscillation was initiated from an idealized state described by the Ekman solution, the SF2010 model produces wind hodographs resembling those of a realistic NLLJ driven purely by geostrophic forcing (see Fig. 1).

Aiming for simplicity and applicability, the VDW2010 model extends the BLK1957 model to include frictional effects, but does so by assuming that the term accounting for divergence of the frictional stress during the transition from day to night and throughout the night remains constant and equal to a hypothetical equilibrium (stationary) nighttime value. The VDW2010 analysis begins with the non-stationary momentum balance equations written as



◀ **Fig. 3** Inertial oscillations calculated over 12-h with BLK1957, SF2010, and VDW2010 models shown respectively from *top to bottom*. In the *left-hand panel* the oscillating profiles show the entire range of wind speed changes during the 12-h simulation (*dashed lines*), while the *black lines* represent the initial wind speed (same for all three models), $\sqrt{u_0^2 + v_0^2}$, and the *solid colored lines* represent the $\sqrt{u^2 + v^2}$ values at hour 12. The *right panels* show the respective hodographs at 250-m height a.g.l. with *dots* indicating equilibrium states (geostrophic for BLK1957 and nighttime Ekman for SF2010 and VDW2010)

$$\frac{\partial u}{\partial t} = f(v - V_g) - \frac{\partial \tau_x}{\partial z}, \tag{11}$$

$$\frac{\partial v}{\partial t} = -f(u - U_g) - \frac{\partial \tau_y}{\partial z}, \tag{12}$$

where τ_x and τ_y are corresponding components of the kinematic turbulent shear stress. As a closure assumption, VDW2010 suggests that the generally time-dependent kinematic turbulent stress divergences can be approximated by time-invariant equilibrium friction terms (i.e., $\frac{\partial \tau_x}{\partial z}(z, t) = F_{xeq}(z)$ and $\frac{\partial \tau_y}{\partial z}(z, t) = F_{yeq}(z)$). These equilibrium stress terms are determined from

$$0 = f(V_g - V_{eq}) + F_{xeq}(z), \tag{13}$$

$$0 = -f(U_g - U_{eq}) + F_{yeq}(z), \tag{14}$$

where $V_{eq}(z)$ and $U_{eq}(z)$ are components of the equilibrium nighttime wind vector. The VDW2010 model thus assumes that the friction during the evening transition is the same as friction in the equilibrium nocturnal boundary layer. Applying this closure in (11) and (12) and integrating the resulting equations over time leads to

$$u - U_{eq} = (v_0 - V_{eq}) \sin ft + (u_0 - U_{eq}) \cos ft, \tag{15}$$

$$v - V_{eq} = (v_0 - V_{eq}) \cos ft - (u_0 - U_{eq}) \sin ft. \tag{16}$$

This solution is shown in the bottom panels of Fig 3. The equilibrium friction terms and thus the equilibrium wind profiles are computed from the Ekman solutions as suggested in VDW2010. In our calculations with the VDW2010 model, the prescribed nighttime eddy viscosity was taken as $5 \text{ m}^2\text{s}^{-1}$. The VDW2010 model yields an oscillation of the wind profile around the nocturnal equilibrium profile. While the oscillation looks more realistic than the one predicted by the BLK1957 model, the VDW2010 assumption of the divergence of frictional stress remaining constant throughout the night is rather artificial. Moreover, this restriction produces a perfectly circular hodograph in contrast to the quasi-spiral shape of the DNS hodograph (see Fig. 1). Also, defining the appropriate equilibrium profiles in the VDW2010 model is problematic as knowing what the equilibrium state would be is not always clear, and the VDW2010 model solution does not tend toward a physical equilibrium state in time.

Upon visual inspection of Fig. 3, one may notice differences between the SF2010 and VDW2010 results. In order to make these differences more visible, the VDW2010 inertial oscillation profiles are superimposed on the SF2010 inertial oscillation profiles in Fig. 4. For both the u - and v -components and the magnitude oscillations, VDW2010 produces a broader oscillation and a higher maximum velocity. The time evolution of differences between the two model predictions is illustrated in Fig. 5. During most of the night, VDW2010 produces higher velocities below 500 m. Overall, the VDW2010 model yields a

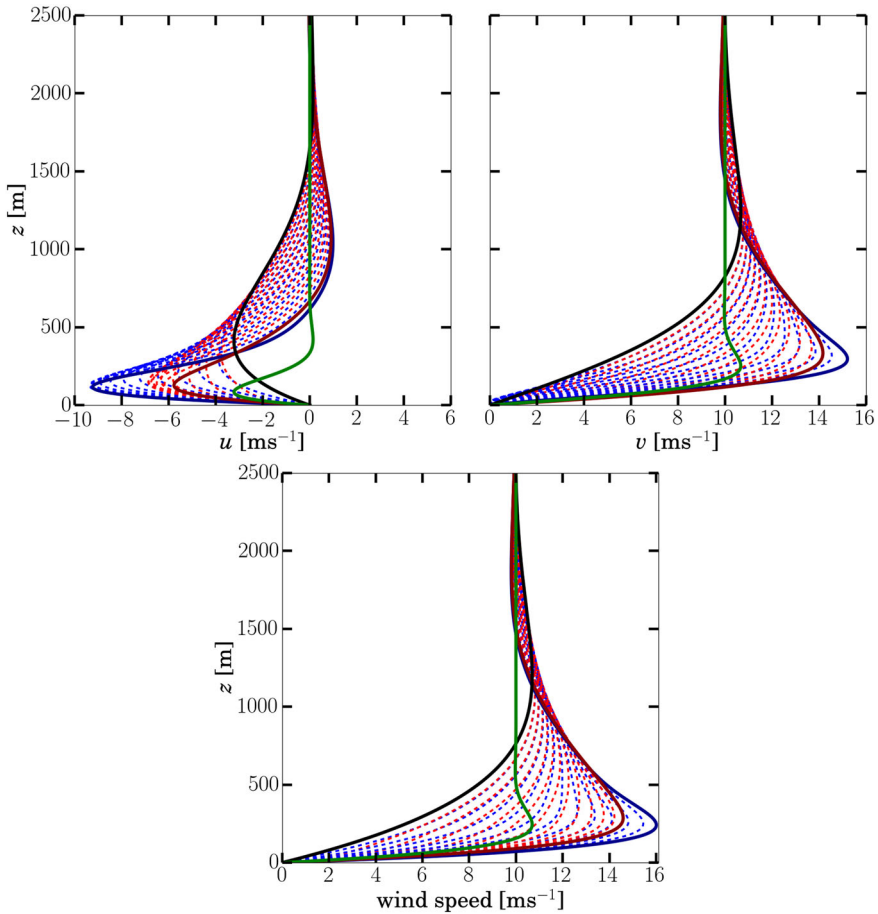


Fig. 4 The SF2010 inertial oscillation over 12-h is shown superimposed on the VDW2010 inertial oscillation over 12-h for comparison. The *upper left panel* shows the *u*-component profiles, the *upper right panel* shows the *v*-component profiles, and the *lower panel* shows the wind magnitude. **Bold black lines** show initial profiles, **red dashed lines** show hourly SF2010 profiles, and **blue dashed lines** show hourly VDW2010 profiles. Corresponding final profiles of the 12-h simulation are shown in **bold red** and **blue lines**. The equilibrium profiles are given by **solid green lines**

jet that is shallower and with a maximum that is closer to the surface compared to the jet predicted by SF2010, but the clearest manifestation of the main difference between the two models can be observed in the hodographs plotted in Fig. 6. At all levels shown, the same tendency is apparent: the VDW2010 hodograph remains at a constant distance from the equilibrium point while the SF2010 hodograph spirals in toward the equilibrium point. The constant curvature radius of the VDW2010 hodograph can be explained upon closer inspection of the VDW2010 equation set. After the substitution of (13) and (14) into (11) and (12), governing flow equations can be written as

$$\frac{\partial(u - U_{eq})}{\partial t} = f(v - V_{eq}), \tag{17}$$

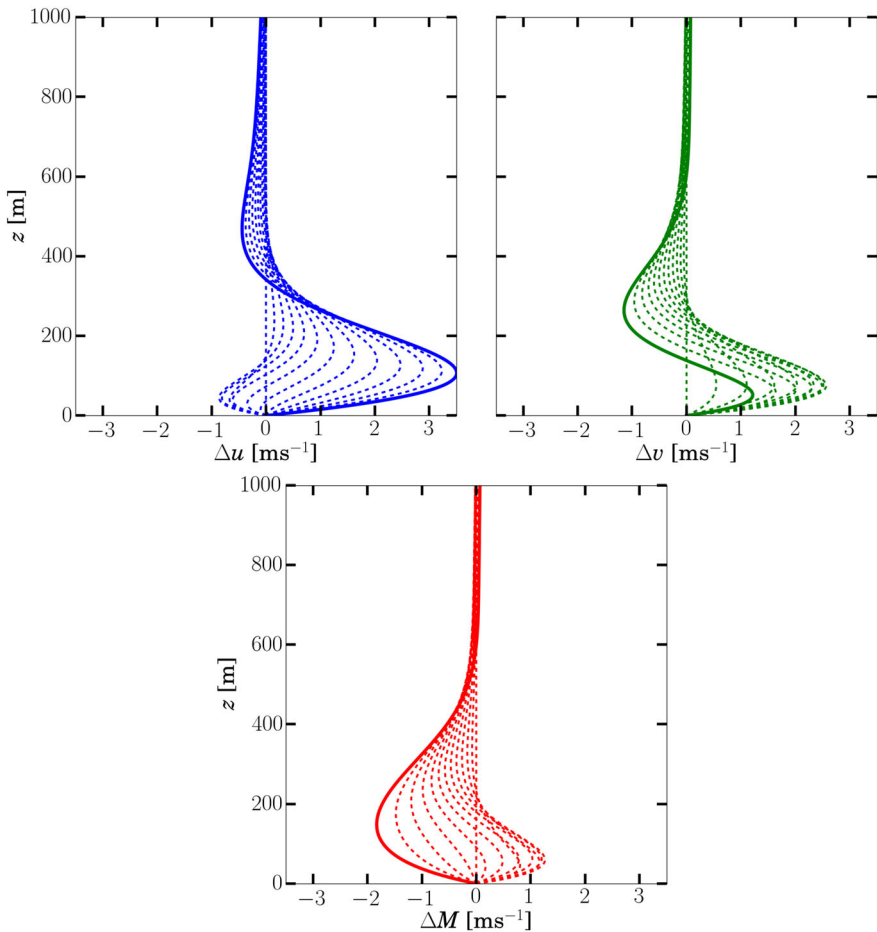


Fig. 5 Vertical profiles of the difference of the SF2010 and VDW2010 models at each hour where $\Delta u = u_{SF} - u_{VDW}$, $\Delta v = v_{SF} - v_{VDW}$, and $\Delta M = \sqrt{u^2 + v^2_{SF}} - \sqrt{u^2 + v^2_{VDW}}$. The *solid line* presents the profile for the final hour of the simulation ($t = 12$ h) while the *dashed lines* indicate the profiles at each hour

$$\frac{\partial(v - V_{eq})}{\partial t} = -f(u - U_{eq}). \tag{18}$$

Multiplying (17) by $(u - U_{eq})$ and (18) by $(v - V_{eq})$, adding the resulting equations together, rearranging terms, and integrating with respect to time leads to

$$(u - U_{eq})^2 + (v - V_{eq})^2 = constant, \tag{19}$$

which is the equation of a circle centered on point (U_{eq}, V_{eq}) . This implies that the oscillation produced by the VDW2010 is fully dependent upon the chosen equilibrium state about which the velocity vector rotates. In the considered case, both analytical approaches were applied within the Ekman model framework, so the equilibrium profile of VDW2010 is identical to the profile toward which SF2010 converges in time.

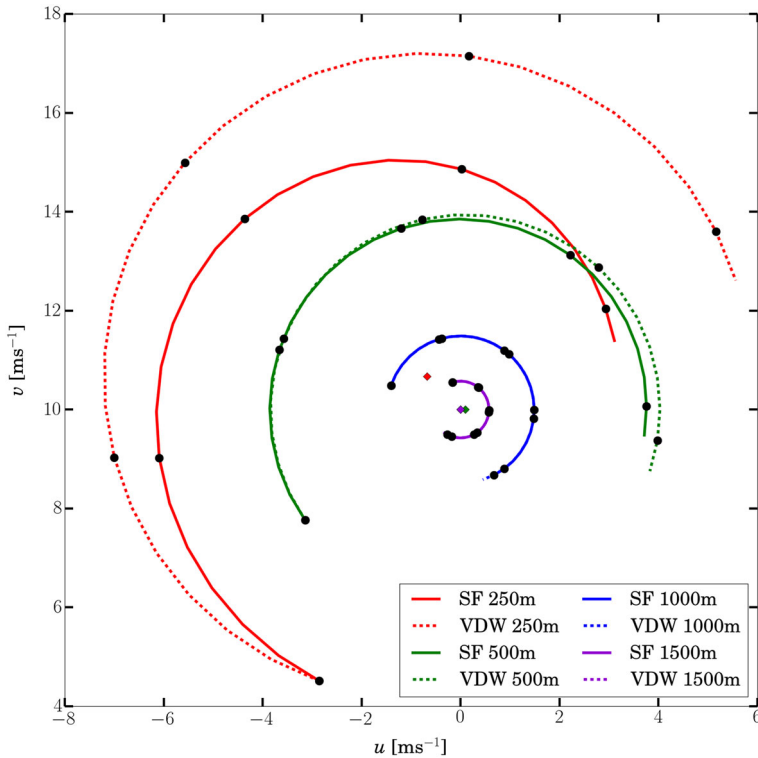


Fig. 6 Wind hodographs obtained with SF2010 (solid lines) and VDW2010 (dashed lines) models at four different heights. Each black dot on the hodographs indicates a 3-h mark

3 Summary

Both the SF2010 and VDW2010 analytical frameworks result in a more realistic jet profile than the BLK1957 model, implying that the inclusion of frictional effects is necessary to produce the NLLJ phenomenon. While the SF2010 model appears to appropriately resolve a jet profile given the idealized Ekman model framework in which it was applied, the simplified approach adopted by the VDW2010 model produces a similar jet profile. The SF2010 model applies an instantaneous drop in eddy viscosity during the transition from day to night allowing the terms accounting for divergence of frictional stress to vary in time through the night. In contrast, the VDW2010 model assumes a constant value for the terms accounting for divergence of frictional stress throughout the night. While the wind profiles appear similar in shape, VDW2010 leads to a jet that is shallower with a lower height of wind maximum compared to SF2010. The SF2010 model leads to a hodograph that has spiral features similar to the spiral hodograph from the DNS run. In contrast, the VDW2010 model yields a circular hodograph.

The dependence of the VDW2010 model solution on the equilibrium-state wind profile implies that a valid method to identify this profile is needed. The authors of VDW2010 [17] recognized this dependence and suggested that an equilibrium profile more realistic than the Ekman model profile should be identified. However, even with a more appropriate equilibrium profile, the VDW2010 model assumption of a constant divergence of frictional

stress would still result in a circular hodograph. In general, the radius of a NLLJ hodograph decreases during the night as implied by the DNS (see Fig 1). While the VDW2010 approach is much simpler than the SF2010 one, it loses much detail in the simplification. This suggests that the VDW2010 method does not adequately describe the NLLJ hodograph in qualitative terms especially at later times. In the case of the SF2010 model, the complexity of its solution could be viewed as a weakness. However, the post-sunset reduction of the eddy viscosity value produces a spiral more consistent with the realistic NLLJ hodographs produced with DNS.

Acknowledgements The authors gratefully acknowledge support through the National Science Foundation (USA) Grant AGS-1359698. The authors are also grateful to anonymous reviewers for their helpful insights on the work.

References

1. Baas P, Bosveld F, Klein Baltink H, Holtslag A (2009) A climatology of nocturnal low-level jets at cabauw. *J Appl Meteorol Climatol* 48(8):1627–1642
2. Banta RM (2008) Stable-boundary-layer regimes from the perspective of the low-level jet. *Acta Geophys* 56(1):58–87
3. Banta R, Newsom R, Lundquist J, Pichugina Y, Coulter R, Mahrt L (2002) Nocturnal low-level jet characteristics over Kansas during cases-99. *Bound Layer Meteorol* 105(2):221–252
4. Beyrich F, Kalass D, Weisensee U (1997) Influence of the nocturnal low-level-jet on the vertical and mesoscale structure of the stable boundary layer as revealed from doppler-sodar-observations. In: *Acoustic remote sensing applications*, Springer, New York, pp 236–246
5. Blackadar AK (1957) Boundary layer wind maxima and their significance for the growth of nocturnal inversions. *Bull Am Meteorol Soc* 38(5):283–290
6. Bonner WD (1968) Climatology of the low level jet. *Mon Weather Rev* 96(12):833–850
7. Ekman VW (1905) On the influence of the earth's rotation on ocean currents. *Ark Mat Astron Fys* 2:1–53
8. Fedorovich E, Shapiro A (2009) Structure of numerically simulated katabatic and anabatic flows along steep slopes. *Acta Geophys* 57(4):981–1010
9. Geurts B (2004) *Elements of direct and large-eddy simulation*. RT Edwards, Philadelphia
10. Hoecker WH Jr (1963) Three southerly low-level jet systems delineated by the weather bureau special pibal network of 1961. *Mon Weather Rev* 91(10):573–582
11. Markowski P, Richardson Y (2011) *Mesoscale meteorology in midlatitudes*. Wiley, New York
12. Mitchell MJ, Arritt RW, Labas K (1995) A climatology of the warm season great plains low-level jet using wind profiler observations. *Weather Forecast* 10(3):576–591
13. Parish TR, Rodi AR, Clark RD (1988) A case study of the summertime great plains low level jet. *Mon Weather Rev* 116(1):94–105
14. Shapiro A, Fedorovich E (2010) Analytical description of a nocturnal low-level jet. *Q J R Meteorol Soc* 136(650):1255–1262
15. Song J, Liao K, Coulter RL, Lesht BM (2005) Climatology of the low-level jet at the southern great plains atmospheric boundary layer experiments site. *J Appl Meteorol* 44(10):1593–1606
16. Stensrud DJ (1996) Importance of low-level jets to climate: a review. *J Clim* 9(8):1698–1711
17. Van de Wiel BJ, Moene A, Steeneveld G, Baas P, Bosveld F, Holtslag A (2010) A conceptual view on inertial oscillations and nocturnal low-level jets. *J Atmos Sci* 67(8):2679–2689
18. Walters CK, Winkler JA, Shadbolt RP, van Ravensway J, Bierly GD (2008) A long-term climatology of southerly and northerly low-level jets for the central united states. *Ann Assoc Am Geogr* 98(3):521–552
19. Whiteman CD, Bian X, Zhong S (1997) Low-level jet climatology from enhanced rawinsonde observations at a site in the southern great plains. *J Appl Meteorol* 36(10):1363–1376
20. Zhong S, Fast JD, Bian X (1996) A case study of the great plains low-level jet using wind profiler network data and a high-resolution mesoscale model. *Mon Weather Rev* 124(5):785–806